

See discussions, stats, and author profiles for this publication at: <https://www.researchgate.net/publication/259722990>

# On the Origin of Increased Sensitivity and Mass Resolution Using Silicon Masks in MALDI

ARTICLE *in* ANALYTICAL CHEMISTRY · JANUARY 2014

Impact Factor: 5.64 · DOI: 10.1021/ac401329r · Source: PubMed

---

CITATION

1

READS

20

## 7 AUTHORS, INCLUDING:



[Julien Franck](#)

Université des Sciences et Technologies de Lill...

53 PUBLICATIONS 884 CITATIONS

[SEE PROFILE](#)



[Maxence Wisztorski](#)

Université des Sciences et Technologies de Lill...

83 PUBLICATIONS 1,267 CITATIONS

[SEE PROFILE](#)



[Cristian Focsa](#)

Université des Sciences et Technologies de Lill...

102 PUBLICATIONS 946 CITATIONS

[SEE PROFILE](#)



[Isabelle Fournier](#)

Université des Sciences et Technologies de Lill...

156 PUBLICATIONS 2,529 CITATIONS

[SEE PROFILE](#)

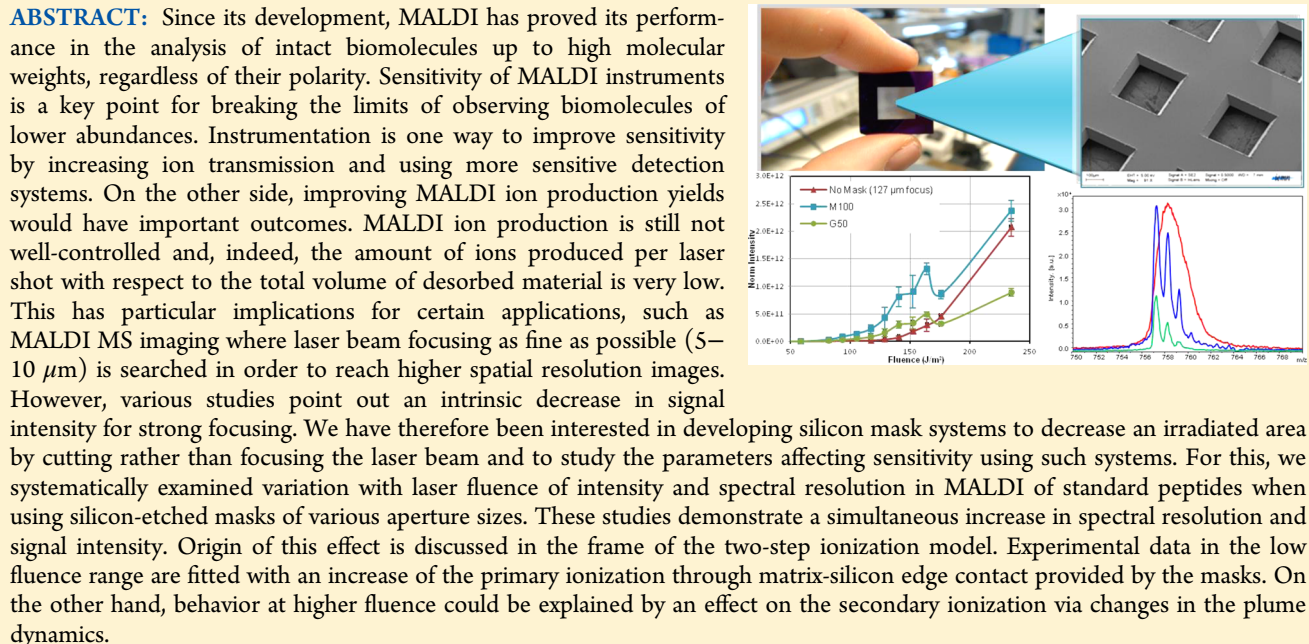
# On the Origin of Increased Sensitivity and Mass Resolution Using Silicon Masks in MALDI

Laurent Diolgent,<sup>†,‡</sup> Julien Franck,<sup>†</sup> Maxence Wisztorski,<sup>†</sup> Anthony Treizebre,<sup>§</sup> Cristian Focsa,<sup>‡</sup> Isabelle Fournier,<sup>\*,†,||</sup> and Michael Ziskind<sup>\*,‡,||</sup>

<sup>†</sup>Laboratoire de Spectrométrie de Masse Biologique Fondamentale et Appliquée - EA 4550, Bât SN3, Université Lille 1, F-59655 Villeneuve d'Ascq Cedex, France

<sup>‡</sup>Laboratoire de Physique des Lasers, Atomes et Molécules - CNRS UMR 8523, Bât P5, Université Lille 1, F-59655 Villeneuve d'Ascq Cedex, France

<sup>§</sup>Institute of Electronics, Microelectronics and Nanotechnology - UMR-CNRS 8520, Université Lille 1, F59655 Villeneuve d'Ascq, France



MALDI<sup>1,2</sup> is nowadays (along with ESI<sup>3,4</sup>) the most widely used method for ion production because of the large variety of analytes accessible by these two techniques. This is particularly true for biomolecule analysis, as demonstrated by the number of studies where these methods are used for various fields of biological applications including proteomics, lipidomics, and metabolomics.

However, despite more than 20 years of successful use and improvement in instrumentation, mechanisms governing ion production in MALDI are still debated in the community. Since MALDI introduction, many efforts were made to study the desorption/ionization process by various means, ranging from experimental observations on conventional systems to the design of specific experiments or theoretical calculations, searching for rationalizing important parameters governing MALDI phenomenon in a unified model. Despite a progressive comprehension of the theory and elaboration of different models<sup>5–9</sup> of MALDI, a clear control on ion production is still

lacking. This leads to important limitations in the sensitivity of MALDI. Indeed, it was shown that ions/ neutrals ratio in the ejected material is extremely low ( $10^{-3}\text{--}10^{-4}$  depending on the experimental conditions<sup>10</sup>), meaning that only very few desorbed molecules will turn to be detectable ions at the end point. Possible increase of ion yields even by a factor of 5–10 is therefore a challenge but would considerably improve analytical performances of MALDI. This has particular implications for certain applications where the amount of analytes might be low, such as certain proteomics analyses or when analyses require high spatial resolution (i.e., small spot size such as  $10\ \mu\text{m}$ ) like for MALDI MS Imaging applications.<sup>11–14</sup> For the latest, spatial resolution has considerably improved over the past years, and images were generated down to a laser spot size of

Received: May 2, 2013

Accepted: January 14, 2014

Published: January 14, 2014

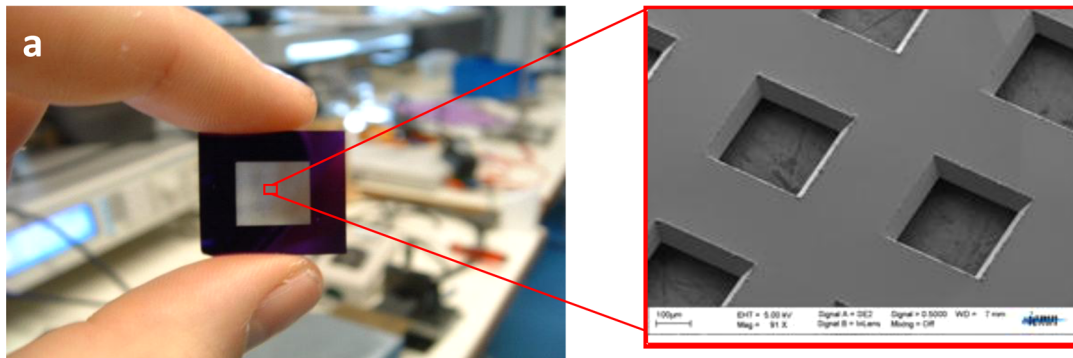


**Figure 1.** (a) Photo of a whole silicon mask and (b) SEM picture zoomed on a portion of the total mask, showing regularly spaced square apertures ( $250\text{ }\mu\text{m}$ ) with the edge perpendicular to the surface of mask.

( $5\text{--}10\text{ }\mu\text{m}$ ).<sup>15–19</sup> Even though many improvements were performed, the low amount of material sampled at this spot size made it difficult to analyze compounds with the lowest representation. Particularly, in such conditions, an increase in signal intensity via an increase in the number of produced ions would be of clear benefit.

We were, thus, interested in studying the evolution of the single intensity with laser fluence for smaller spot size. For this purpose, we searched for a simple, low cost system that we could easily use on various MALDI mass spectrometers and that could provide access to various spot sizes. We chose to develop silicon wafer masks that can be applied on top of the sample to decrease the irradiated area by simply cutting out the incident laser beam instead of using a conventional system for increasing laser focusing. We tested masks systems on two MALDI-TOF instruments and studied the evolution of ion signal (intensity and spectral resolution) with laser fluence and spot size. Several geometries of masks were studied and, interestingly, we observed that for certain mask geometries, the signal was not only maintained to its original intensity but even increased. Here, we systematically studied this effect in order to elucidate its possible origin and determine to what extent we could obtain an increase in signal intensity.

## ■ EXPERIMENTAL SECTION

**Masks Manufacturing.** Masks realized with silicon substrate  $\langle 100 \rangle$  of  $200\text{ }\mu\text{m}$  of thickness, structured by DRIE (deep reactive ion etching) have been used.<sup>20</sup> It consists of a series of etching steps with  $\text{SF}_6$  gases and passivation with  $\text{C}_4\text{F}_8$  gases. The passivating steps are used to protect the side faces of structures during the etching step so that it occurs only in the depth direction. The etching rate obtained under these conditions is  $4\text{ }\mu\text{m}/\text{min}$ . Twelve micrometers thickness of photosensitive resin layer AZ9260 is used to protect the areas not etched. The realized masks are  $60\text{ }\mu\text{m}$  thick with square apertures of various side dimensions of  $25, 50, 100, 250$ , and  $500\text{ }\mu\text{m}$ . In this manufacturing procedure, the apertures present straight edges, perpendicular to the wafer section. For each wafer, network apertures were made according to a defined raster. For conventional masks, this raster was created to obtain apertures spaced by about  $120\text{--}150\text{ }\mu\text{m}$  side-to-side. For certain experiments, masks with apertures spaced by shorter distances ( $10\text{--}20\text{ }\mu\text{m}$  side-to-side) were designed, and these were referred to as mask arrays. On one wafer, we can manufacture up to 9 of these rasters, whatever the distance between apertures (conventional mask or mask array) (Figure 1). For conventional masks with  $150\text{ }\mu\text{m}$  distance between

apertures, the distance matches the laser spot diameter and allows the irradiation of a single aperture. For mask arrays, since the distance is much shorter than the laser diameter, several apertures are irradiated during one experiment.

**MALDI MS Analysis.** **MALDI-TOF Analysis.** For analysis on the MALDI-TOF instrument (Voyager DE-STR Elite, Applied BioSystems, Framingham, MA), MALDI samples were prepared from aqueous solutions of standard peptides, including bradykinin ( $m/z$  1060,  $5.10^{-6}\text{ mol/L}$ ) and bovine insulin ( $m/z$  5734,  $5.10^{-5}\text{ mol/L}$ ). For these experiments,  $\alpha$ -cyano 4-hydroxycinnamic acid (HCCA) at a concentration of  $20\text{ mg/mL}$  in acetone (saturated solution) was used as the matrix. Samples were deposited according to either the dried droplet or thin layer<sup>21</sup> preparation methods and deposited onto an ITO glass slide mounted on a sample plate and allowed for microscopic observation. Briefly, for thin layer preparation,  $1\text{ }\mu\text{L}$  of matrix solution was deposited on the support and  $1\text{ }\mu\text{L}$  of analyte solution was added on top of the dried matrix layer. For dried droplet preparation,  $1\text{ }\mu\text{L}$  of analyte solution was deposited on the ITO slide and  $1\text{ }\mu\text{L}$  of matrix solution was added on top before sample crystallization. In both preparations, the sample was left to dry at RT. The thin layer preparation was used to ensure the production of highly homogeneous samples in terms of crystal density.

Masks were maintained on top of the sample preparation using a brass thin plate showing a window the size of the wafer and placed above it. This brass plate was itself fixed on the ITO glass slide using a double side conductive tape carbon adhesive tab (Euromedex). This setup allows the mask to be positioned on top of the glass slide, serving as a sample support making a direct contact between the mask and the sample preparation. Mass spectra were acquired on the MALDI-TOF instrument in the positive linear mode using an extraction delay of  $100\text{ ns}$  and an acceleration voltage of  $25\text{ kV}$ . These parameters optimize the analyte peak intensity in the mass spectra recorded without a mask. The incident angle of the used laser to the normal of the sample plate is  $45^\circ$ .

**MALDI-TOF/TOF Analysis.** For the experiments performed on the MALDI-TOF/TOF instrument (Ultraflex II, Bruker Daltonics, Bremen, Germany), the Pepmix powder (Bruker Daltonics, Bremen, Germany) was reconstituted in  $150\text{ }\mu\text{L}$  of  $\text{H}_2\text{O}$  (TFA 0.1%) and then equally mixed with a solution of HCCA at  $10\text{ mg/mL}$  in  $\text{AcN}/\text{H}_2\text{O}$  (TFA 0.1%) (7:3, v/v). The solution was manually sprayed at the surface of an ITO glass slide using an electrospray nebulizer attached to a  $500\text{ }\mu\text{L}$  syringe, and the flow rate was set to  $4.2\text{ }\mu\text{L}/\text{min}$ . The nebulizer was moved uniformly throughout the center of the ITO glass

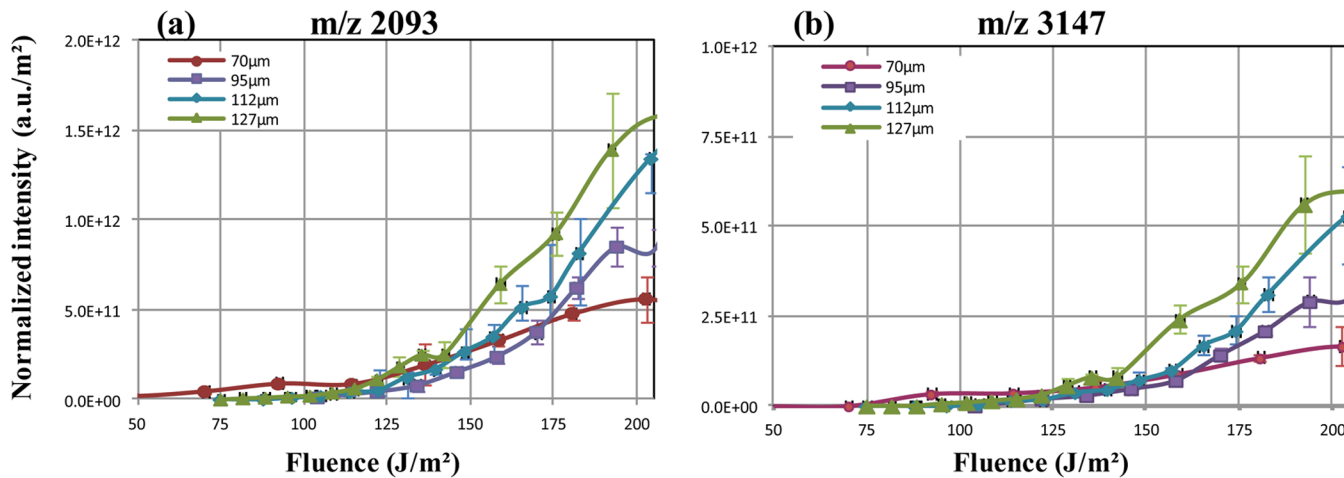


**Figure 2.** Evolution with laser fluence of the analyte signal intensity (normalized to the spot area) recorded on the MALDI-TOF/TOF Ultraflex II system for two different analytes and four different spot sizes: 127, 112, 95, and 70  $\mu\text{m}$ . (a) Protonated signal of ACTH Clip (1–17) at  $m/z$  2093 and (b) protonated signal of Somatostatin at  $m/z$  3147. Vertical bars indicate the RMS.

slide by covering an area of approximately 4  $\text{cm}^2$  for 45 min to ensure uniform matrix-pepmix application.

Masks presenting an aperture size of 50 and 100  $\mu\text{m}$  were then consecutively placed at the surface of the homogeneous layer of the matrix-pepmix layer. The sample was then analyzed using the Ultraflex II mass spectrometer equipped with a Smart beam (355 nm, third harmonic of a Nd:YAG laser) having a repetition rate up to 200 Hz and an incidence angle of 60° to the normal of the sample plate. This laser has a specific energy profile, homogeneous on time average, since it is patterned by a rotating grid in order to provide many rotating high-energy points in the profile (see Holle and co-workers<sup>22</sup>). The MALDI-TOF/TOF ion source is constituted by two extraction regions, enabling it to work in the delayed extraction mode. In order to optimize spectral resolution, voltages applied on the plate and the first extraction grid are adjustable, as well as the delay time. The focusing system of the instrument is made by Einzel lenses located just after the second extraction grid of the ion source. The instrument is equipped with a two stages reflectron but mass spectra were recorded in linear positive mode and were averaged on 200 laser shots per aperture at the mass range of  $m/z$  0–4500, a delayed extraction of 150 ns, and a frequency of 100 Hz. Four different laser focusing regimes preset in the instrument were used. For all laser spot dimensions, the energy was increased from 0 to 100%, considering the following settings: offset 65 and range 35. The voltages for the ion source 1, ion source 2, and lens were set at 25, 23.65, and 6.45 kV, respectively, with a delayed extraction of 100, 150, and 250 ns.

All experiments were conducted in triplicate, and the resulting mass spectra were processed using FlexAnalysis 3.0 (Bruker Daltonics, Bremen, Germany). A baseline subtraction was applied on all mass spectra and for the  $m/z$  757 ( $[\text{M} + \text{H}]^+$  ion signal of Bradykinin (1–7)),  $m/z$  2093 ( $[\text{M} + \text{H}]^+$  ion signal of ACTH Clip (1–17)), and  $m/z$  3147 ( $[\text{M} + \text{H}]^+$  ion signal of Somatostatin).

**Laser Spot Diameter Measurement.** For all laser focusing regimes, the corresponding spot dimensions were measured after irradiation of a thin matrix layer of HCCA. For this, a saturated solution of HCCA in pure acetone was prepared and applied on an ITO glass slide. Sample was irradiated at the four different focuses preset in the instrument (large, medium, small,

and minimum) with and without masks. Samples were irradiated just above the threshold for analyte ion detection until the matrix layer was totally removed. The ablated area was measured with a  $\times 5$  magnification under a Zeiss Axioskop (Zeiss, Germany) microscope equipped with an AxioCam MRC digital camera (Zeiss, Germany) and controlled by Axiovision 4.8.2 (Zeiss, Germany). In addition, near field laser profile with and without the mask was recorded using a beam profiler (Beamage Gentec-EO, Canada).

When the laser wavelength and the typical dimensions of the mask (aperture size and mask thickness, the latter giving the distance between the mask and the target) is taken into account, the Fresnel number is around 100 for both Voyager DE-STR and Ultraflex II. For this value, the laser intensities are relatively homogeneous along their surfaces (but even more for the Ultraflex II: quasi top-hat profile). One can, therefore, disregard any diffraction phenomenon, as confirmed by the near field profiles (data not shown).

## RESULTS AND DISCUSSION

### Preliminary Study: Laser Spot Size Dependence.

Existence of four different focusing regimes of the laser beam for the MALDI-TOF/TOF gives access to the study of the signal intensity for the protonated ion of the three tested peptides with respect to the laser fluence. Figure 2 shows the evolution of the signal intensity normalized to the laser spot area for  $m/z$  2093 and  $m/z$  3147. These distributions are in good agreement with previous experiments carried out on similar instruments.<sup>22</sup> They are also in line with previous experiments performed where signal intensity dependence with laser spot size was studied.<sup>10,23,24</sup> In particular, slopes ( $m$ ) of the normalized ion intensities versus fluence curve ( $I_0 \propto F^m$ ) are found to be smaller for smaller laser spots than those for larger ones:  $m = 3.5$  for a diameter of 70  $\mu\text{m}$ ,  $m = 9$  for a diameter of 127  $\mu\text{m}$ , regardless of the recorded ion. This confirms the signal decrease is more important than expected by simple reduction of the laser spot size, by 1 to 3 orders of magnitude, depending on the laser profile.<sup>23</sup>

**Spatial Resolution.** Figure 3 shows examples of matrix layer removal after irradiation of the sample at high laser fluence through masks of different apertures on the Voyager DE-STR Elite. The corresponding desorbed areas are largely

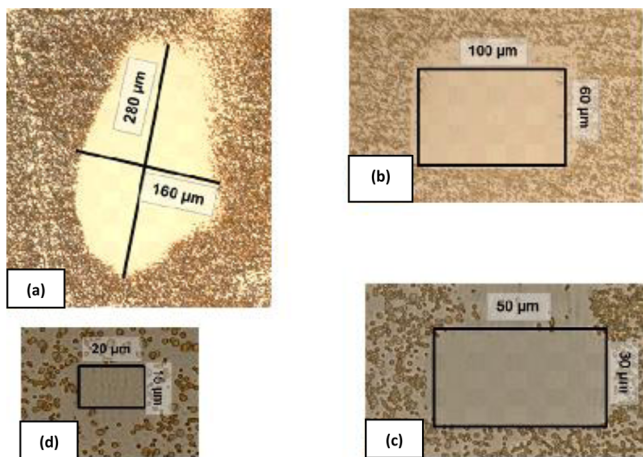


**Figure 3.** Desorbed area observed after irradiation of an HCCA thin layer ( $1 \mu\text{L}$  of saturated solution in acetone) (a) without mask; through a mask of  $60 \mu\text{m}$  thickness and (b)  $100 \mu\text{m}$ , (c)  $50 \mu\text{m}$ , and (d)  $25 \mu\text{m}$  square aperture size.

reduced (by a factor of  $\sim 3$  to  $100$  in the provided examples of Figure 3, panels b, c, and d) with respect to those obtained without masks ( $275 \times 150 \mu\text{m}$  spot size, see Figure 3a). However, their shapes are rectangular rather than square as the width of the depleted area is smaller than expected. For instance, the  $25 \times 25 \mu\text{m}^2$  aperture leads to a cleaned surface of  $\sim 20 \times 15 \mu\text{m}^2$ . This discrepancy is obviously due to the laser beam incidence angle of  $45^\circ$ . Thus the system [mask + target] leads to the occurrence of a shadow area (i.e., a region of the target which is not irradiated) of which one can easily take

profit to further improve the spatial resolution (see Figure 4). However, the dimensions of the shadow area are generally smaller than calculated by taking the mask geometries and the laser incidence angle. Indeed, calculations would lead to expect shadow areas of  $60\%$  for  $100 \mu\text{m}$  aperture size and  $100\%$  for  $25$  and  $50 \mu\text{m}$  aperture sizes. This deviation has been attributed to the reflection of the beam by the inner edge of the mask to the sample. When this effect is taken into account, the estimation of the irradiated surface becomes comparable to the observed ablated surface for  $50$  and  $100 \mu\text{m}$  aperture sizes after a single reflection, while two reflections are required to account for the ablated surface for the  $25 \mu\text{m}$  aperture size. At this point, it should be underlined that the reflectance of the silicon at  $337 \text{ nm}$  is estimated to  $\sim 50\%$ , but the high laser fluence used in the experiments described in this section ensures the complete depletion of the layer, even after multireflection.

For the Ultraflex II mass spectrometer, for which spot dimensions can be changed, the irradiated areas were determined by examination of the remove material from a thin layer preparation after irradiation. These experiments show that irradiated areas show a quasi-circular shape for the 4 different preadjusted focuses of the instrument, leading to the determination of diameters of  $70 \mu\text{m}$  (presetting minimum),  $95 \mu\text{m}$  (presetting large),  $112 \mu\text{m}$  (presetting small), and  $127 \mu\text{m}$  (presetting medium), respectively. When masks are applied on the sample, similar observations to those obtained with the Voyager Elite can be made. However, the larger angle of incidence ( $60^\circ$ ) for this instrument induces an increased shadow area. By taking into account the incidence angle of the laser and the masks geometry, we expect that under  $\sim 105 \mu\text{m}$  aperture size, the sample should not be irradiated directly by

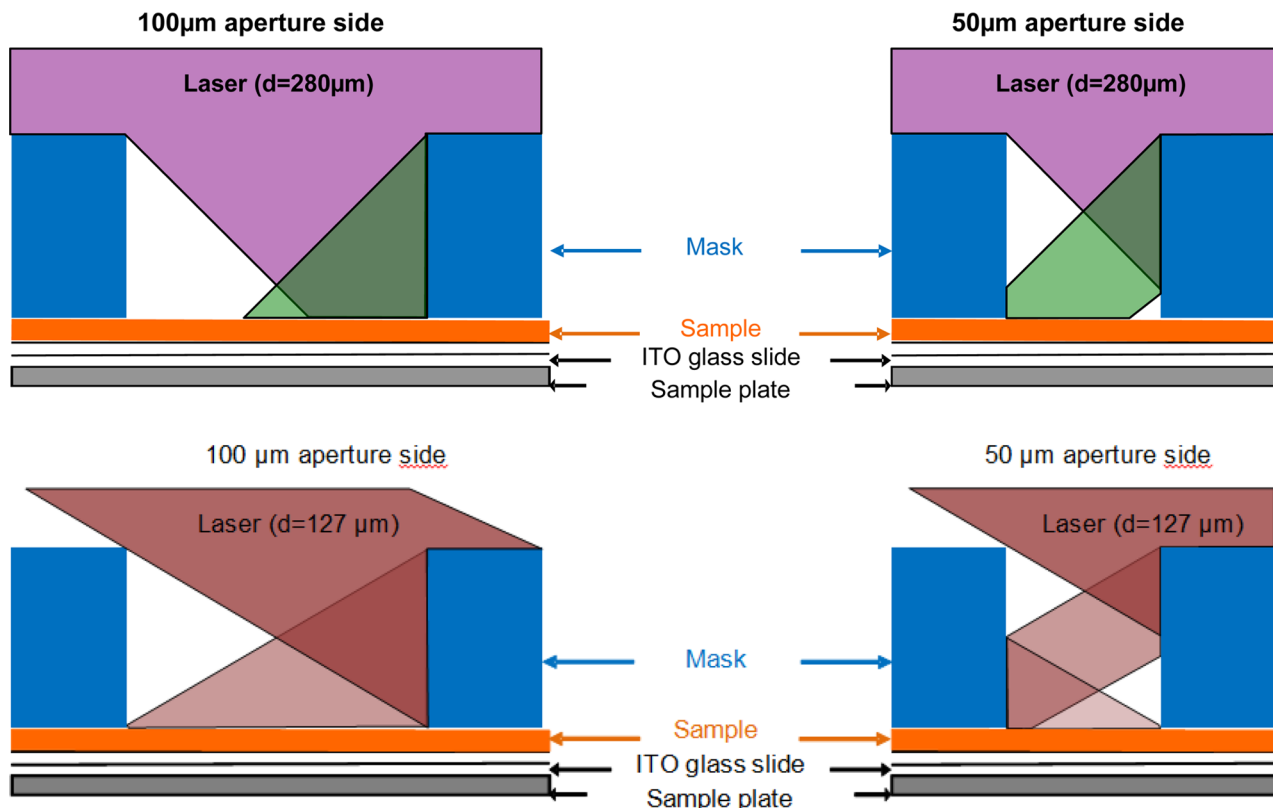


**Figure 4.** Schematic representation of the mask system and the reflection on the walls due to the laser beam angle of incidence (up:  $45^\circ$  incidence angle for the Voyager instrument configuration and down:  $60^\circ$  incidence angle for the Ultraflex instrument configuration).

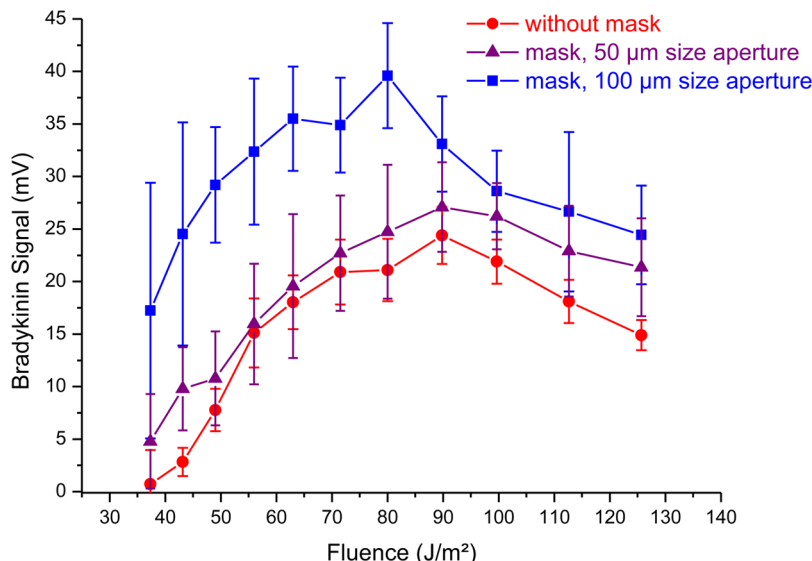


**Figure 5.** Evolution with laser fluence of the protonated analyte signal intensity (here Bradykinin) recorded on the MALDI-TOF Voyager instrument for masks of 50 µm (M50) and 100 µm (M100) aperture size and 60 µm thickness, and a comparison to signal evolution without the mask system. Vertical bars indicate the RMS.

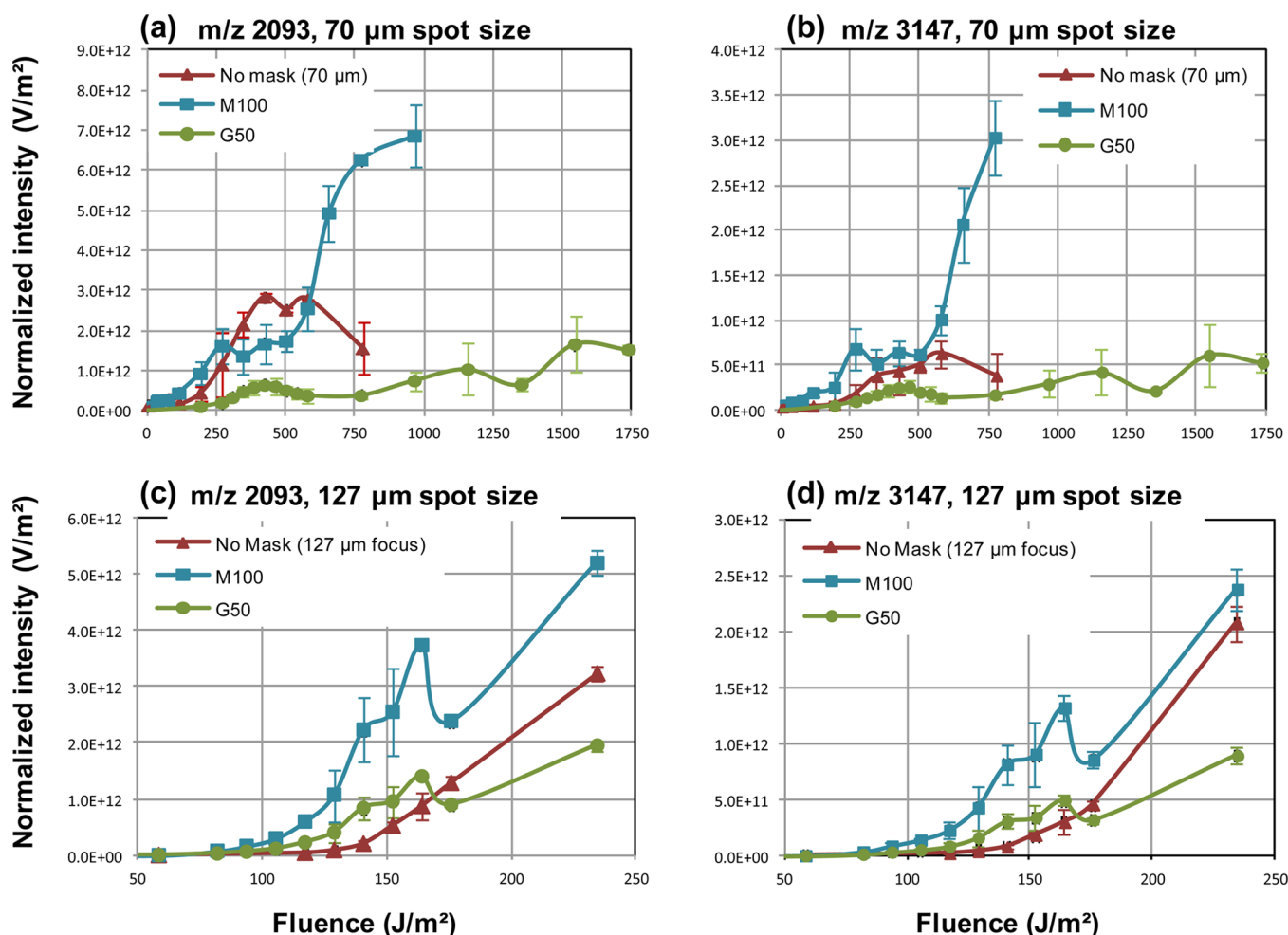


**Figure 6.** Evolution with laser fluence of the analyte signal intensity (normalized to the spot area) recorded on the MALDI-TOF/TOF Ultraflex II system for two different spot sizes (127 and 70 µm) and two different analytes with a 100 µm aperture mask (M100), a 50 µm aperture mask array (G50), and without a mask. (a and c) Protonated signal of ACTH Clip (1–17) at  $m/z$  2093 for laser spot size of (a) 70 µm and (c) 127 µm. (b and d) Protonated signal of Somatostatin at  $m/z$  3147 for laser spot size of (b) 70 µm and (d) 127 µm. Vertical bars indicate the RMS.

the laser (this holds for most configurations). However, for 100  $\mu\text{m}$  aperture size masks, we observed rectangular ablation areas of  $\sim 100 \mu\text{m}$  length (about the size of the aperture) and  $\sim 35 \mu\text{m}$  in width. Similarly, 50  $\mu\text{m}$  aperture size masks show ablated areas of  $\sim 50 \mu\text{m}$  in length and  $\sim 45 \mu\text{m}$  in width. Again, material removal can only be explained if one takes into account beam reflection(s) on the mask inner walls. For this laser incidence angle, one reflection can be expected for 100  $\mu\text{m}$  and two for 50  $\mu\text{m}$ . Calculations lead to expected areas roughly similar to those experimentally observed.

**Sensitivity.** Figure 5 shows the evolution of protonated bradykinin peak intensity with increasing laser fluence on the Voyager DE-STR Elite during the irradiation of HCCA-bradykinin sample, directly or through masks of 50 and 100  $\mu\text{m}$  aperture sizes. Every reported value corresponds to an average of 10 measurements obtained at different sample locations. Fluence has been chosen in the range of standard MALDI analysis (i.e., just above the threshold for ion production). In principle, the fluence should be recorded directly on the target (i.e., behind the mask systems) to compare the distributions. Indeed, in the absence of reflection, this parameter is independent of the mask configuration since the irradiated energy and the spot size decrease in the same way when the aperture width is reduced (photons density is preserved). However, since the reflectance of the silicon mask is not 100% (50% according to measurement performed on a Silicon wafer), (multi)reflection of the laser beam on the wall of the mask should normally decrease the fluence at the bottom of the aperture. The complexity of the measurement leads us to record the laser fluence in front of the mask. This will be considered in the following text.

The global aspect of all fluence distributions of analyte is similar, regardless the mask configuration, and can be interpreted using the commonly accepted two-step MALDI ionization model, initially developed by Bökelmann<sup>25</sup> and then developed by Knochenmuss and Zenobi,<sup>26</sup> also referred as coupled photophysical and chemical dynamics (CPCD) by Knochenmuss in his more recent work.<sup>27</sup> Briefly, above the ion-production threshold, protonated matrix ions are massively generated or released by primary ionization processes (i.e., during the laser irradiation). Together with desorbed neutrals, clusters, and other minority ions, they form a desorbed plume dense enough to initiate efficient secondary ionization by proton transfer reactions via collisions between the protonated matrix and neutral analyte. On the other hand, at laser fluence about 2–3 times above the threshold, saturation, and then a decrease of the analyte signal<sup>6,24</sup> is observed. This is not related to ion fragmentation only as one could presume and not necessarily fitting with a model assuming reaction equilibrium in the plume. Such a behavior is observed for HCCA and different CCA derivatives such as Cl-CCA, as demonstrated in the work of Soltwisch et al., where they studied the ion yield dependence on laser wavelength and energy for several matrices.<sup>7</sup> This is also found by Knochenmuss et al. in their recent paper where they use the CPCD as a model for wavelength and matrix dependence of the MALDI mechanism. The decrease in analyte signal intensity would thus be related to the specific plume characteristics for CCA derivatives due to the absorption cross-section leading to faster pooling processes and slower secondary reaction kinetics.<sup>27</sup>

Surprisingly, the use of masks improves in many circumstances the sensitivity of the analysis (i.e., the intensity of the analyte peak). For instance, while the irradiated area is about

20× smaller, the protonated bradykinin signal intensity recorded with the 50  $\mu\text{m}$  aperture size is comparable to that obtained without the mask. The use of 100  $\mu\text{m}$  aperture size increases it by  $\sim 50\%$  with respect to the most intense peak recorded without the mask. On the other hand, spectra recorded with the smallest aperture (25  $\mu\text{m}$ ) show analyte signals generally less intense by only a factor of 2 or 3. When the spatial resolution enhancement ( $\times 100$ ) is taken into account, this decrease remains very moderate. These trends remain the same for Bovine insulin (and peptide mixtures), despite the high dispersion of measurements likely due to the heterogeneity of the analyte distribution when the irradiated area is lower than  $\sim 100 \times 100 \mu\text{m}^2$ .

Figure 6 shows the evolution of the normalized intensity (normalization to the ablated area) of the  $[\text{M} + \text{H}]^+$  ion signals of ACTH Clip (1–17) ( $m/z$  2093) and Somatostatin ( $m/z$  3147) with the laser fluence of the Ultraflex II, directly or through masks of 100  $\mu\text{m}$  aperture sizes or through a mask array of a 50  $\mu\text{m}$  aperture (see below). For these experiments, we examined the smallest and largest laser spot size accessible (i.e. 70 and 127  $\mu\text{m}$ ). Note that for some configurations, the diameter could be smaller than the aperture size of the mask, which means that only the shadowing effect contributes to reduce the irradiated area. Despite the many differences of configuration between the Voyager Elite and the Ultraflex II, the use of the mask again has a positive effect on the sensitivity. For 127  $\mu\text{m}$  at low fluence, the effect is well-marked for all peptide ions. For 70  $\mu\text{m}$ , the effect is more remarkable for higher fluences ( $> 500 \text{ J/m}^2$ , far from the typical MALDI range) and the highest  $m/z$ . This points out that the positive effect observed using the mask is not associated to a peculiar configuration of the MALDI mass spectrometer (such like the ion transmission, the electric field, the laser profile, etc.) but to the desorption/ionization process itself. Finally, in the low fluence range (below  $\sim 150 \text{ J/m}^2$ ), all the distributions are superimposed as in the case of the Voyager DE-STR Elite. By contrast, at higher fluence (not measured with the Voyager), they evolve differently with and without the mask. In particular, one or several bumps are evidenced, always at the same fluences, in all the distributions recorded when masks are used. This is more pronounced at 175  $\text{J/m}^2$  with a 127  $\mu\text{m}$  spot size (see Figure 6, panels c and d).

Complementary studies have been performed to provide insight into the cause of these unexpected effects. First, absence of signal in the irradiation through masks of pure bradykinin sample excludes mechanisms related to matrix-free laser desorption/ionization technique such as DIOS (desorption/ionization on silicon), based on the deposition of pure analytes on submicrometric porous silicon surface.<sup>28–31</sup> The sensitivity enhancement has thus to be explained within the framework of the MALDI technique (i.e., via increasing matrix ion yield or protonated matrix-neutral analyte interaction). Some observations seem to strengthen the direct role of the primary ionization. In particular, the relative gain in sensitivity occurs at fluence close to the ion production threshold, in a range where the ablation plume is not dense and the secondary ionization processes not very efficient. This observation has to be connected to the remarkable decrease of ion production threshold for masked studies, slight for 50  $\mu\text{m}$  aperture size and pronounced for 100  $\mu\text{m}$ . This result strongly contrasts with those obtained by focusing the laser spot (see above).

A primary ionization mechanism partly consistent with our study could be linked to the existence of a photoelectric effect

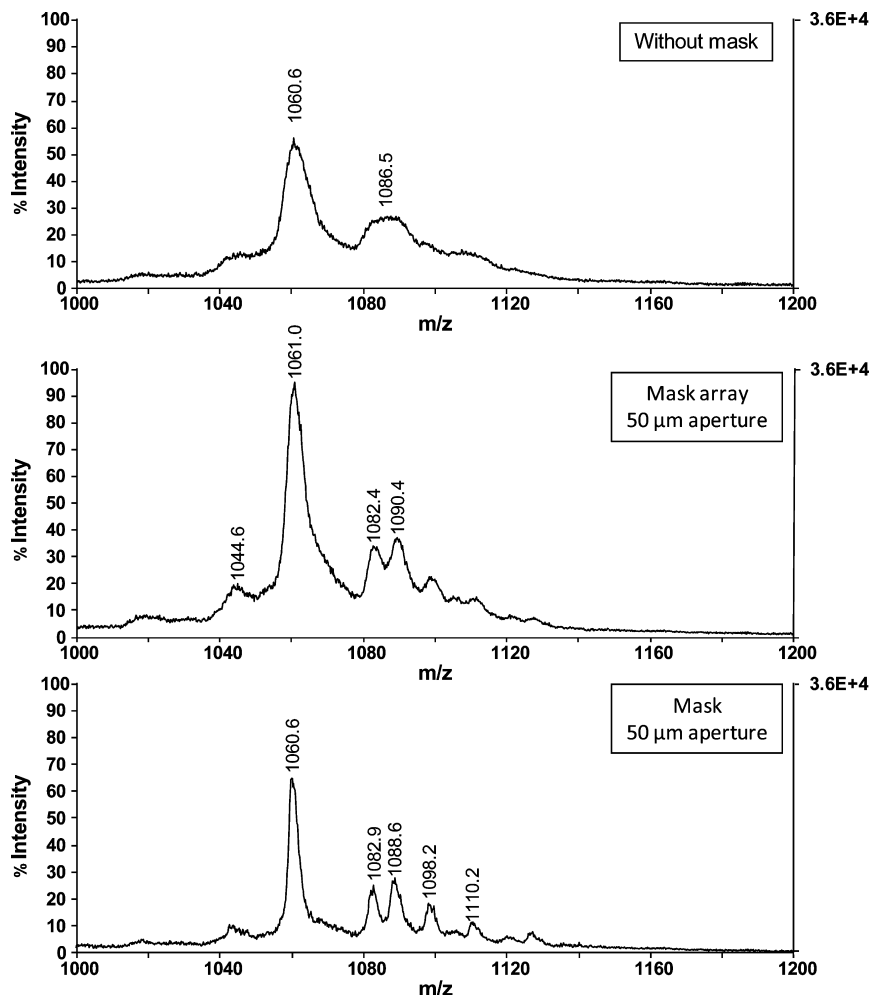


**Figure 7.** Zoomed view in the  $m/z$  range corresponding to the signal of bradykinin of the MALDI-TOF MS spectra recorded in the linear positive mode (laser fluence:  $80 \text{ J/m}^2$ ). Spectra were recorded for a single mask and a mask array of the same thickness ( $60 \mu\text{m}$ ) and aperture size ( $50 \mu\text{m}$ ) and were compared to a spectrum obtained without a mask system.

on the fraction of sample in contact with the silicon edge of the mask. Following the surface-enhancement matrix photoionization model proposed by McCombie and Knochenmuss<sup>32</sup> to describe the ion yields of thin samples deposited on metal substrate, the presence of matrix within tunneling range of the metal (or the semiconductor in our case) leads to the coupling of matrix and substrate molecular orbitals. Consequently, the highest occupied and the lowest unoccupied molecular orbitals (HOMO and LUMO) of the matrix are shifted. If the resulting LUMO orbital drops beyond the Fermi level of the substrate, it is populated, leading to a decrease of the gap to the ionization potential of the matrix down to the work function. With regard to the laser wavelength (337 nm, 3.7 eV), the tested HCCA matrix ionization potential (8.5 eV) and the work function of pure silicon (4.6 eV),<sup>33</sup> two photons could efficiently ionize the matrix layer in contact with the edge of the mask, while three photons are necessary to ionize matrix present in the bulk. The result is a decrease of the ionization threshold. Thus, at low fluence, the primary ionization enhancement effect could only involve this matrix layer. The layer may originate from two sources. The first one corresponds to the fraction of the matrix present in the early stage of the plume, which simultaneously interacts with the silicon edges and the tail of the laser pulse. Taking account of the typical velocity of the plume (600 m/s)<sup>34–36</sup> and the laser pulse duration (10 ns), one can estimate

that the height of the layer is a few micrometers, whereas its section obviously has the dimension of the aperture. The second possible source corresponds to desorption, and then the deposition of a matrix film on the Si mask walls after every laser pulse. The next pulse(s) will then irradiate this layer together with the sample. Note that in these scenarios, the energy brought by the laser to the sample should be sufficient to initiate the ejection of neutral material to form a desorption plume or a matrix layer on the walls of the apertures. This is highly likely since the desorption threshold is usually far below the ion production threshold.

Some experiments and observations support these assumptions. First, the fluence distributions of two thin layers of analytes deposited respectively onto the standard ITO glass and onto a silicon wafer have been compared (without mask). The results clearly demonstrate a decrease of the ion production threshold and an enhancement of the signal when the silicon substrate is used. Not surprisingly, this positive effect is limited to the low fluence range.

Furthermore, analyte signal is quite undetectable in mass spectra recorded using the Voyager setup with masks of the V-shaped aperture (tilted walls with  $50^\circ$  angle to the mask section) produced through chemical etching of the same wafers. This could be associated with the forward peaking in the angular distribution of the ejected material, which drastically

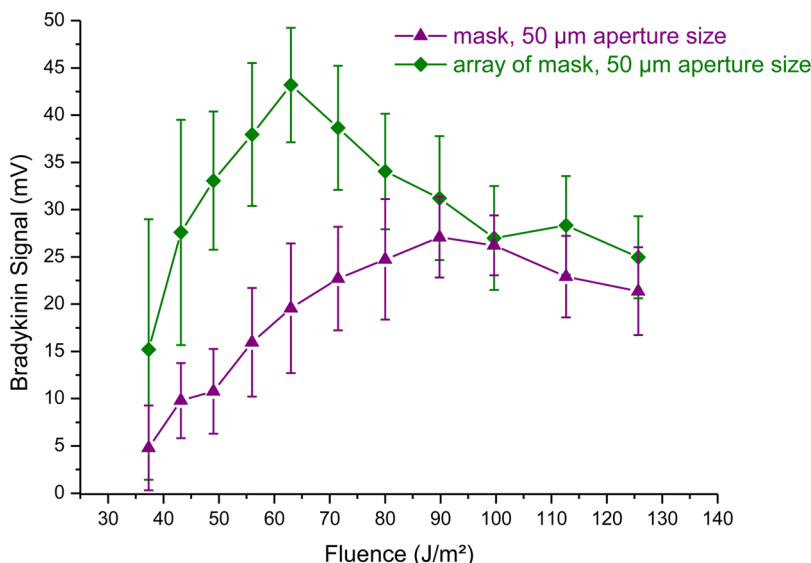


**Figure 8.** Evolution with laser fluence of the analyte signal intensity (here Bradykinin) for a single mask and a mask array of same thickness ( $60\ \mu\text{m}$ ) and aperture size ( $50\ \mu\text{m}$ ). Vertical bars indicate the RMS.

reduced the contact of the matrix layer with the oblique walls of this type of mask.

On the other hand, the proposed mechanism could at least partially explain some interesting trends evidenced in the fluence distributions. For instance, the superposition of all the distributions below  $150\ \text{J}/\text{m}^2$  is a clear indication that reflection on the silicon wall of the mask is negligible in the low fluence range (i.e., all the energy of the laser pulse is used to ablate the layer). Otherwise, the distributions recorded with mask should be shifted, since partial reflection of the laser beam on the wall of the mask should decrease the fluence. This is in good agreement with our model where the ablation/ionization is achieved from a layer in contact with the mask rather than from the bottom of the aperture. At higher laser fluence, the inflection and occasionally the decrease evidenced in the distributions recorded through masks could be explained by the removal of the layer during the pulse duration, by faster pooling processes and slower secondary reaction kinetics, or by increased fragmentation of the material ablated from the wall (not evidenced in the mass spectra). However, high laser fluence could also lead to reflection from a part of the beam to the bottom of the sample, leading to the ejection of fresh material. Finally, the new increase of the signal after the bump could be the result of these two opposite mechanisms. In this frame, the oscillation of the signal with increasing fluence evidenced for the smallest apertures (or grid, see G50 in Figure 7, panels a and b) could be associated to a second reflection, as depicted in the bottom-right Figure 4. The less homogeneous profile of the laser and the small range of available fluence probably prevent similar observations with the Voyager Elite. However, the sudden increase of the signal evidenced in Figure 6 (panels a and b) at highest fluence (above  $500\ \text{mJ}/\text{m}^2$ ) cannot be explained by this mechanism alone. One cannot exclude at this stage that the walls of the mask could also lead to the confinement of the plume. This could induce an amplification of ion/molecule collisions in the plume due to a more favorable thermodynamic equilibrium and consequently to a better proton exchange between matrix ions and analytes. Finally, the improved sensitivity at high energy could at least partially be the result of this secondary ionization enhancement.

This assumption is supported by the previous observations on the V-shape mask. Nevertheless, the confinement effect alone could not explain the superposition of the distributions at low fluence (since a reflection is expected in this case).

Finally, the increased sensitivity at low fluence could originate from a surface-enhancement matrix photoionization effect, while the global increase in intensity at high fluence may have its origin in a change in the plume dynamics affecting the kinetics of secondary reactions. A superposition of these two different effects is expected in a certain range of fluence, depending on the characteristic dimensions of the mask and on the geometry of the laser beam (profile, incidence angle).

Further experiments using different mask material (including metal and insulator) and thickness, and complementary investigation on the dynamics of the plume by ICCD camera fast imaging are required to discriminate between these different mechanisms.

**Mass Resolution.** Figure 7 shows a zoom of mass spectra centered on the protonated and cationized bradykinin ion signals and recorded with and without a mask, using the Voyager Elite mass spectrometer. It is clearly evidenced that the use of the mask also enhances the mass resolution. This gives, for instance, the possibility to completely dissociate the peaks corresponding to the bradykinin adducts. Note that other parameters generally used to improve the resolution (e.g., extraction delay, acceleration, and reflector voltages) have been optimized for the detection of signal in the absence of any mask, giving possibilities of further enhancement.

By contrast with the sensitivity, this effect is more accurate for smallest aperture and high fluence (but in the normal range of a standard analysis). More precisely, enlargement of the analyte peak with increasing fluence is much less pronounced with a mask. Thus, mass resolution improvement does not exactly coincide with the sensitivity enhancement, which could suggest different origins for the two effects. It is well-known that the mass peak broadening observed in the linear mass spectra is mainly caused by the kinetic energy and longitudinal spatial distributions of the formed ions, which turns in the spread of the ions traveling through the drift region of the mass spectrometer. In the case of a MALDI TOF-MS, one only

needs to take the energy spread into account, since generation of ions is always achieved close to the sample surface. In view of these considerations, a possible explanation could be that the shape of the laser beam turns to a more homogeneous profile after it has been cut by the mask. The entire matrix is then irradiated with the same laser fluence, conferring a narrower fluence distribution to the desorbed ions. In this frame, the more homogeneous beam profile of the Ultraflex II naturally leads to a more modest improvement of the mass resolution. However, we observed a very different behavior according to the spot size chosen. For the 127  $\mu\text{m}$  spot size and 150 ns delay time, a resolution of  $R_s = 1340$  is calculated for  $m/z$  757. Equivalent spectral resolution of  $R_s = 1340$  is calculated for 100  $\mu\text{m}$  aperture mask (M100), while  $R_s$  is found to be 1850 and 1410 for masks of 50  $\mu\text{m}$  aperture (M50) and array of mask of 50  $\mu\text{m}$  aperture (G50), respectively. The resolution is again higher for M50 than M100 or G50, which is in line with our results from the Voyager Elite. The main difference is that the increase of resolution is lower on the Ultraflex II. For 70  $\mu\text{m}$  spot size and identical delay, curiously we observe a drastic decrease in the spectral resolution from  $R_s = 1340$  down to  $R_s = 240$  for  $m/z$  757, meaning that isotopic pattern is no more observable. With the use of M100 and G50, an important increase is observed and  $R_s$  is measured to be  $R_s = 1150$  and  $R_s = 1500$ , respectively. This effect is observed on the whole standard fluence range. Remarkably, the masks or array of masks allow for the compensation of the resolution loss at this spot size. Again G50 shows higher increase than M100, as we previously observed on the Voyager Elite instrument. Similar behavior was observed for other delays (e.g., 100 and 250 ns).

This recalls the use of a spatially structured laser beam profile to improve MALDI performance.<sup>22</sup> Note that in this work, mass resolution enhancement leads to increased sensitivity, while these two phenomena are decoupled here.

**Mask Array.** By sufficiently reducing the distance between some apertures, one can form a mask array. Consequently, the laser pulse simultaneously irradiates several apertures. Since a bigger surface is affected, the mask array should provide a further increase of the sensitivity compared to a single mask but at the cost of spatial resolution deterioration. The benefit in sensitivity is clearly demonstrated by the Figure 8, which shows the comparison of the fluence distributions of bradykinin signal during the irradiation of sample through the 50  $\mu\text{m}$  aperture mask and the corresponding array (distance between two apertures: 25  $\mu\text{m}$ ). However, while nine apertures are simultaneously irradiated by the laser, the intensity of the bradykinin peak only increases by a factor of 4 at most. This result can be interpreted in the continuation of our previous explanation. Each sample region is irradiated by a quasi top-hat laser beam but with a different fluence because of the Gaussian profile of the laser beam before the array: high fluence for the central aperture and lower fluence for the periphery. In this frame, the fluence distribution results from the convolution of nine distributions shifted to each other. This also explains the alteration of the mass resolution (albeit, it is still superior to that obtained without a mask, see Figure 7). Another possibility is that collisions between the different plumes could have a counter-productive effect on the production of analyte ions. This could explain the sudden fall of the signal at high laser fluence. Plume imagery studies are necessary to determine the plume divergence and check this assumption. Finally, the nanophotonic enhancement or the polarization dependence of the ion yield evidenced in the work of Vertes group on arrays of

pillars<sup>37,38</sup> and the behavior models from capillary-like restricted volumes by Knochenmuss<sup>39</sup> are not expected here because of the dimensions of our arrays, much larger than the laser wavelength used.

In the case of the Ultraflex II, the diameters of the laser beam limit the number of irradiated apertures to one or two at most. No increase of the sensitivity compared to a simple mask is then expected. In fact, if a positive effect is still observed with the mask array of 50  $\mu\text{m}$  apertures for 127  $\mu\text{m}$  spot size, the effect is lower than those observed for the 100  $\mu\text{m}$  single aperture. For the 70  $\mu\text{m}$  spot size, no more positive effect is observed, but for 70  $\mu\text{m}$  this would actually lead to a configuration closer to the 50  $\mu\text{m}$  single aperture mask. However, mask array remains useful since it facilitates the delicate positioning of the inclined beam inside the smallest apertures and justifies its application in the study of the sensitivity with the Ultraflex II.

## CONCLUSION

Systematic studies on model peptides using various mask configurations, laser fluences, and spot sizes demonstrated a positive effect of the use of masks on signal intensity and spectral resolution. Using such masks, we are able to observe an increase of signal intensity along with an improvement (up to a factor of 100) of the spatial resolution for specific configurations. This effect is more pronounced for certain aperture dimensions. Interestingly, mask geometries giving the highest increase in sensitivity are not the ones allowing for the highest increase in spectral resolution to be reached, therefore demonstrating that the two effects are decoupled. In other studies (data not shown), where masks showing V-shaped apertures were used, the effect was observed to be far less marked compared to square aperture masks presented here.

In the frame of the two-steps ionization model<sup>5</sup> (or coupled photophysical and chemical dynamics model<sup>27</sup>), this effect could come either from an increase in the first or from an increase in the second ionization step. Our results and previous studies are consistent with an increase in the primary ionization step (matrix ions production) at low fluence due to interaction with the silicon mask. On the other hand, at higher fluence they are also in line with an increase in the secondary ionization step (analyte ion production) by change in the plume dynamics and kinetics of secondary reactions through plume confinement. We assume that these two effects coexist and combine together, pushing in the same positive direction for ion formation. In order to confirm which of the mechanisms is involved, it could be interesting to test masks made out of different materials, although such masks may be difficult to realize. Another interesting perspective for this work would be to test the masks on an instrument equipped with a coaxial laser and with finer focusing (i.e., 5–10  $\mu\text{m}$ ), in order to determine if these effects are still observed for small spot sizes.

Finally, these mask systems could find interesting applications for MALDI analysis since they can easily be adjusted on the majority of commercial MALDI mass spectrometer without any major structure modifications of the instrument and could allow a clear gain in signal intensity, especially for higher molecular weights.

## AUTHOR INFORMATION

### Corresponding Authors

\*E-mail: isabelle.fournier@univ-lille1.fr. Tel: +33 (0)3 20 43 41 94, Fax: +33 (0)3 20 43 40 54.

\*E-mail: michael.ziskind@univ-lille1.fr. Tel: +33 (0)3 20 33 63 30, Fax: +33 (0)3 20 33 64 63.

### Author Contributions

<sup>†</sup>I.F. and M.Z. contributed equally.

### Notes

The authors declare no competing financial interest.

### ACKNOWLEDGMENTS

Supported by grants from University Lille 1 (Ph.D. grant to L.D.), Ministère de l'Enseignement Supérieur et de la Recherche via Institut Universitaire de France (IUF Junior grant to I.F.), and the National Agency for Research ANR (ANR Blanche FUN MALDI, 2008).

### REFERENCES

- (1) Karas, M.; Hillenkamp, F. *Anal. Chem.* **1988**, *60*, 2299–2301.
- (2) Karas, M.; Bachmann, D.; Bahr, U.; Hillenkamp, F. *Int. J. Mass Spectrom. Ion Processes* **1987**, *78*, 53–68.
- (3) Fenn, J. B.; Mann, M.; Meng, C. K.; Wong, S. F.; Whitehouse, C. M. *Science* **1989**, *246*, 64–71.
- (4) Yamashita, M.; Fenn, J. B. *J. Phys. Chem.* **1984**, *88*, 4451–4459.
- (5) Knochenmuss, R.; Zenobi, R. *Chem. Rev.* **2003**, *103*, 441–452.
- (6) Dreisewerd, K. *Chem. Rev.* **2003**, *103*, 395–425.
- (7) Soltwisch, J.; Jaskolla, T. W.; Hillenkamp, F.; Karas, M.; Dreisewerd, K. *Anal. Chem.* **2012**, *84*, 6567–6576.
- (8) Knochenmuss, R.; Zhigilei, L. V. *Anal. Bioanal. Chem.* **2012**, *402*, 2511–2519.
- (9) Knochenmuss, R. *Analyst* **2006**, *131*, 966–986.
- (10) Dreisewerd, K.; Schuerenberg, M.; Karas, M.; Hillenkamp, F. *Int. J. Mass Spectrom. Ion Processes* **1995**, *141*, 127–148.
- (11) Caprioli, R. M.; Farmer, T. B.; Gile, J. *Anal. Chem.* **1997**, *69*, 4751–4760.
- (12) Gagnon, H.; Franck, J.; Wisztorski, M.; Day, R.; Fournier, I.; Salzet, M. *Prog. Histochem. Cytochem.* **2012**, *47*, 133–174.
- (13) Spengler, B.; Hubert, M.; Kaufmann, R. *MALDI Ion Imaging and Biological Ion Imaging with a New Scanning UV-Laser Microprobe*, Proceedings of the 42nd Annual Conference on Mass Spectrometry and Allied Topics, 1994, Chicago, Illinois, May 29–June 3, 1994; p 1041.
- (14) Stoeckli, M.; Farmer, T. B.; Caprioli, R. M. *J. Am. Soc. Mass Spectrom.* **1999**, *10*, 67–71.
- (15) Deutskens, F.; Yang, J.; Caprioli, R. M. *J. Mass Spectrom.* **2011**, *46*, 568–571.
- (16) Roempp, A.; Spengler, B. *Histochem. Cell Biol.* **2013**, *139*, 759–783.
- (17) Rompp, A.; Guenther, S.; Schober, Y.; Schulz, O.; Takats, Z.; Kummer, W.; Spengler, B. *Angew. Chem., Int. Ed.* **2010**, *49*, 3834–3838.
- (18) Spengler, B.; Hubert, M. *J. Am. Soc. Mass Spectrom.* **2002**, *13*, 735–748.
- (19) Zavalin, A.; Yang, J.; Caprioli, R. *J. Am. Soc. Mass Spectrom.* **2013**, *24*, 1153–1156.
- (20) Abdolvand, R.; Ayazi, F. *Sens. Actuators, A* **2008**, *144*, 109–116.
- (21) Vorm, O.; Roepstorff, P.; Mann, M. *Anal. Chem.* **1994**, *66*, 3281–3287.
- (22) Holle, A.; Haase, A.; Kayser, M.; Hohndorf, J. *J. Mass Spectrom.* **2006**, *41*, 705–716.
- (23) Guenther, S.; Koestler, M.; Schulz, O.; Spengler, B. *Int. J. Mass Spectrom.* **2010**, *294*, 7–15.
- (24) Qiao, H.; Spicer, V.; Ens, W. *Rapid Commun. Mass Spectrom.* **2008**, *22*, 2779–2790.
- (25) Bökelmann, V.; Spengler, B.; Kaufmann, R. *Eur. J. Mass Spectrom.* **1995**, *1*, 81–93.
- (26) Zenobi, R.; Knochenmuss, R. *Mass Spectrom. Rev.* **1999**, *17*, 337–366.
- (27) Knochenmuss, R. *Analyst* **2014**, *139*, 147–156.
- (28) Wei, J.; Buriak, J. M.; Siuzdak, G. *Nature* **1999**, *399*, 243–246.
- (29) Chen, Y.; Vertes, A. *Anal. Chem.* **2006**, *78*, 5835–5844.
- (30) Zhang, Q.; Zou, H.; Guo, Z.; Zhang, Q.; Chen, X.; Ni, J. *Rapid Commun. Mass Spectrom.* **2001**, *15*, 217–223.
- (31) Nayak, R.; Knapp, D. R. *Anal. Chem.* **2007**, *79*, 4950–4956.
- (32) McCombie, G.; Knochenmuss, R. *J. Am. Soc. Mass Spectrom.* **2006**, *17*, 737–745.
- (33) Knochenmuss, R.; McCombie, G.; Faderl, M. *J. Phys. Chem. A* **2006**, *110*, 12728–12733.
- (34) Gluckmann, M.; Karas, M. *J. Mass Spectrom.* **1999**, *34*, 467–477.
- (35) Puretzky, A. A.; Geohegan, D. B.; Hurst, G. B.; Buchanan, M. V.; Luk'yanchuk, B. S. *Phys. Rev. Lett.* **1999**, *83*, 444–447.
- (36) Karas, M.; Bahr, U.; Fournier, I.; Gluckmann, M.; Pfenninger, A. *Int. J. Mass Spectrom.* **2003**, *226*, 239–248.
- (37) Walker, B. N.; Razunguzwa, T.; Powell, M.; Knochenmuss, R.; Vertes, A. *Angew. Chem., Int. Ed.* **2009**, *48*, 1669–1672.
- (38) Stolee, J. A.; Walker, B. N.; Zorba, V.; Russo, R. E.; Vertes, A. *Phys. Chem. Chem. Phys.* **2012**, *14*, 8453–8471.
- (39) Knochenmuss, R. *Eur. J. Mass Spectrom.* **2009**, *15*, 189–198.